Sensors & Actuators: B. Chemical 276 (2018) 95–100

Contents lists available at ScienceDirect

Sensors and Actuators B: Chemical

journal homepage: www.elsevier.com/locate/snb

Modulation of assembly and disassembly of a new tetraphenylethene based nanosensor for highly selective detection of hyaluronidase

Xiangqian Li[a], Zhan Zhou[b,**], Yiping Tang[c], Cheng Cheng Zhang[d], Yuhui Zheng[a], Jinwei Gao[e], Qianming Wang[a,c,*]

[a] Key Laboratory of Theoretical Chemistry of Environment, Ministry of Education, School of Chemistry & Environment, South China Normal University, Guangzhou 510006, China
[b] College of Chemistry and Chemical Engineering, Henan Key Laboratory of Function-Oriented Porous Materials, Luoyang Normal University, Luoyang 471934, PR China
[c] College of Material Science and Engineering, Zhejiang University of Technology, Hangzhou, Zhejiang, 310014, China
[d] Departments of Physiology and Developmental Biology, University of Texas, Southwestern Medical Center, Dallas, TX 75390-9133, USA
[e] Guangdong Provincial Engineering Technology Research Center For Transparent Conductive Materials, South China Normal University, Guangzhou 510006, China

ARTICLE INFO

Keywords:
Hyaluronidase
Aggregation induced emission
Sensor

ABSTRACT

The development of nanoprobes with high sensitivity and specificity for tumor marker detection has gained increasing attention in biological applications. Here, we have designed and synthesized a novel 4,4',4",4"'-(ethene-1,1,2,2-tetrayltetrakis(benzene-4,1-diyl))tetrakis (1-(4-bromobenzyl)pyridin-1-ium) bromide (TPE-4N$^+$) based aggregation induced emission (AIE) fluorescent sensor and it gives rise to electrostatic adsorption towards hyaluronic acid (HA), resulting in an effective emission recovery in yellow-greenish region. In the presence of hyaluronidase (HAase), the enzymatic digestion between HA and HAase induces the fluorescence quenching and this "*on-off*" change has been analyzed by two consecutive linear equations. The low detection limit is determined to be 0.02 U/mL by quantitative evaluation and its practical application has been verified by detecting human urine samples. It is promising that this new approach can be utilized to study a wide variety of other depolymerization reactions.

1. Introduction

As a polymeric host with excellent water solubility, hyaluronic acid (HA), an anionic glycosaminoglycan, is composed of repeating d-glucuronic acid and N-acetyl-d-glucosamine and exists in human tissues or living cells [1]. Hyaluronidase (HAase) plays an essential role for degrading HA in the process of cancer cell metastasis. It has been investigated that HAase is relevant to a variety of physiological and pathological processes, including embryogenesis, inflammation, wound healing and over express in certain patients with cancers (such as bladder, colon or prostate) [2]. Therefore, the evaluation of HAase activity in cells has received considerable interests since it may be served as a tumor marker [3,4]. Traditional methods for hyaluronidase detection like turbidimetry [5], viscosimetry [6] and colorimetry [7] have been studied. However, many of these approaches have relatively poor selectivity, low sensitivity, and require relatively complicated devices. Therefore, it will be of great significance to develop simple, rapid, and sensitive methods for detection of HAase.

Aggregation induced emission (AIE) is an unexpected fluorescent effect (a type of propeller-shaped molecule, which emits faintly in their solutions but fluoresce intensely in the aggregated state), which was reported in year 2001 [8]. Among the AIE luminogens, tetraphenylethene (TPE) and its derivatives have been extensively studied because of their simple synthetic routes, easy functionalization, notable AIE performance and high fluorescence quantum yield [9–14]. They have been grafted onto organic compounds and covalent polymers working as functional building blocks, fluorescent sensors or solid-state materials during the past decades [15–18]. Especially in the field of chemical and biological detection, various AIE based fluorescent probes were designed and prepared for sensitively detection of metal ions, sugars, proteins or anions and so on [19–23].

Here, we have synthesized a novel AIE molecule (TPE-4N$^+$) using a simple one-step substitution reaction between tetrakis(4-pyridylphenyl) ethylene and 4-bromobenzyl bromide. Subsequently, HA was attached

* Corresponding author at: Key Laboratory of Theoretical Chemistry of Environment, Ministry of Education, School of Chemistry & Environment, South China Normal University, Guangzhou 510006, China.
** Corresponding author.
E-mail addresses: zhouzhan@lynu.edu.cn (Z. Zhou), qmwang@scnu.edu.cn (Q. Wang).

https://doi.org/10.1016/j.snb.2018.08.093
Received 24 April 2018; Received in revised form 16 August 2018; Accepted 20 August 2018
Available online 22 August 2018

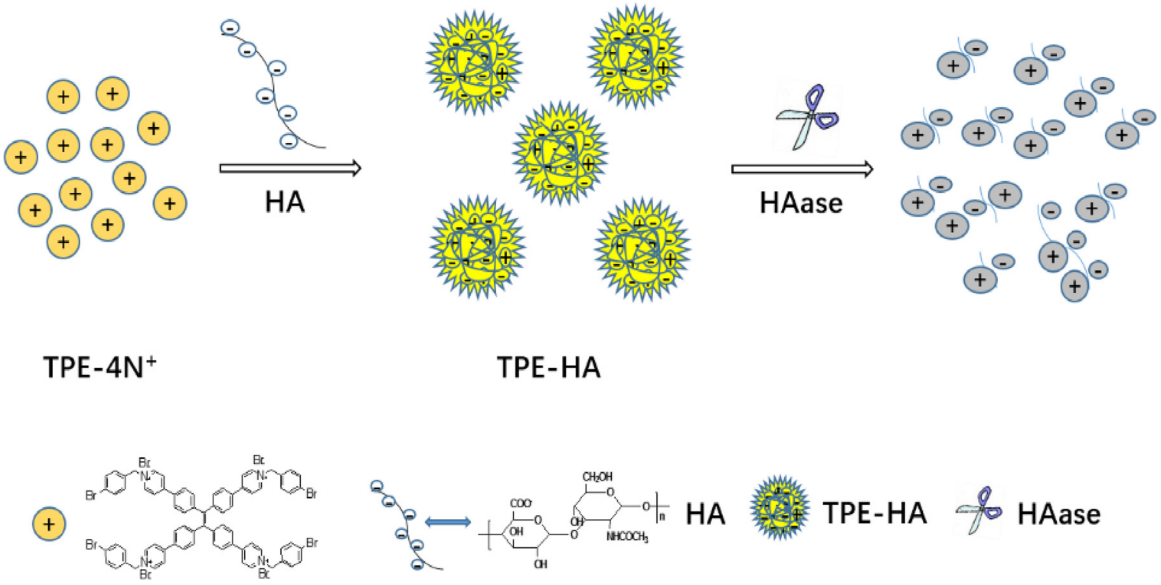

Fig. 1. Schematic illustration of TPE-HA based fluorescence nanoprobe for detection of HAase.

to the surface of TPE-4N$^+$ molecule via their electrostatic interactions to assemble the uniform nanoparticles (TPE-HA). The aggregated TPE-HA displayed a strong emission at 536 nm in the aqueous solution, while its fluorescence was dramatically suppressed upon addition of HAase. The results showed that HAase could be specific and effectively degrade HA and reduce the electrostatic interactions between TPE-4N$^+$ and HA. This charge change can induce the disassembly of TPE-HA, leading to the fluorescence quenching in the system. The luminescence evolution can be realized with bare eye observation under the irradiation of a portable UV lamp. Hence, TPE-HA can be applied as a nanochemosensor for the detection of HAase in the aqueous solution (Fig. 1). It is anticipated that the nanoprobe could be acted as a diagnostic and monitoring material under biological and environmental conditions.

2. Experimental sections

2.1. Reagents and materials

Tetrakis (4-pyridylphenyl) ethylene (98%), 4-Bromobenzyl bromide (98%), dichloromethane (99.9%), acetonitrile (99.9%), hyaluronic acid (HA, 97%), hyaluronidase (HAase, 308 U/mg), glutathione (GSH, 98%), L-cysteine (Cys, 99%), homocysteine (Hcy, 95%), glutamic acid (Glu, 99%), ascorbic acid (AA, 98%), alkaline phosphatase (ALP, > 10,000 U/L), urea (UA, 99%), vitamin B1 (VB1, 99%) and bovine serum albumin (BSA, 98%) were purchased from Aladdin Chemistry Co. Ltd. Metal salts such as Copper chloride ($CuCl_2$), Ferric chloride ($FeCl_3$), Zinc chloride ($ZnCl_2$), Magnesium chloride ($MgCl_2$) were purchased from Guangzhou Chemical Reagent Factory and used without further purification.

2.2. Apparatus

^{1}H NMR spectra were recorded on a Bruker Avance 400 MHz NMR Spectrometer (Bruker, Karlsruhe, Germany). TEM images were obtained with a JEOL JEM-2100HR transmission electron microscope (Hitachi Ltd, Japan). The particle size distribution and Zeta potentials was determined by Malvern Nano-ZS90 were acquired by a particle size analyzer and ZetaPlus Zeta Potential Analyzer (Malvern Instruments Ltd, United Kingdom). UV–vis spectra were recorded on TECHCOMP spectrophotometer in the range of 230–600 nm with a slit of 2 nm (TECHCOMP Ltd, Shanghai, China). Fluorescence and excitation spectra were measured using a Hitachi F-7000 fluorescence spectrophotometer with a 150 W xenon lamp as a light source (Hitachi Ltd, Japan). All error bars represent standard deviations from three repeated experiments.

2.3. Synthesis and characterization of TPE-4N$^+$

Tetrakis(4-pyridylphenyl)ethylene (0.156 mmol, 100 mg) and 4-bromobenzyl bromide (0.624 mmol, 282.2 mg) were dissolved in the mixture solution of CH_3CN (25 mL) and CH_2Cl_2 (25 mL). Then, the mixture was refluxed at 120 °C for 3 days under N_2 atmosphere. The reaction mixture was concentrated by rotary evaporation and washed using dichloromethane for several times. A yellow powder was obtained by filtration, and dried under vacuum at room temperature for 8 h. The structure and synthesis procedure of TPE-4N$^+$ were shown in Fig. S1. ^{1}H NMR (400 MHz, d_{DMSO}) δ (ppm) 9.19–9.17 (8H, d, J = 8 Hz), 8.49–8.47 (8H, d, J = 8 Hz), 7.98–7.96 (8H, d, J = 8 Hz), 7.68–7.66 (8H, d, J = 8 Hz), 7.52–7.50 (8H, d, J = 8 Hz), 7.36–7.33 (8H, d, J = 12 Hz), 5.80 (8H, s) (Fig. S2).

2.4. HAase detection based on the TPE-HA Nanosystem

For HAase detection in aqueous solution, TPE-4N$^+$ (1 μM) and HA (0.15 μg mL^{-1}) were mixed with different amounts (0–5 U/ml) of HAase in 1 mL of pure water solution in a spectrophotometer quartz cuvette. After incubation at 37 °C for 100 min, the spectra were measured and collected by a fluorescence spectrophotometer excited at 348 nm. For comparison purpose, control experiments were performed by replacing HAase with other interfering analytes GSH, Cys, Hcy, Glu, AA, UA, VB1, BSA, $CuCl_2$, $FeCl_3$, $ZnCl_2$, $MgCl_2$ (10 μM) or 0.1 U/mL ALP under identical conditions.

2.5. Detection of HAase in urine samples

Human urine samples from two healthy people were provided by Guangdong Provincial Hospital of Chinese Medicine (Guangzhou, China). The urine samples were purified by high centrifugation (12,000 rpm) for 10 min, then the supernatant was transferred into the several vials (2 mL) and adjusted to pH = 4.3 (NaH_2PO_4, Na_2HPO_4 and NaCl buffer). For HAase detection in urine samples, the fluorescence measurements were recorded for the samples containing TPE-HA nanosystem (TPE-4N$^+$ 1 μM, HA 0.15 μg mL^{-1}). The emission intensity at 536 nm was measured and the concentration of HAase was calculated

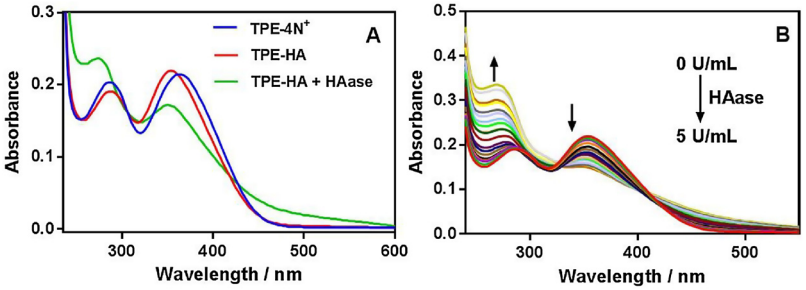

Fig. 2. (A) UV–vis spectra for TPE-$4N^+$ (1 μM), TPE-HA (TPE-$4N^+$ 1 μM, HA 0.15 μg mL^{-1}) and TPE-HA (TPE-$4N^+$ 1 μM, HA 0.15 μg mL^{-1}) + HAase (5 U/mL) in aqueous solution. (B) UV–vis absorbance changes by gradually adding HAase (from 0 to 5 U/mL) into TPE-HA (TPE-$4N^+$ 1 μM, HA 0.15 μg mL^{-1}) aqueous solution (All the samples were incubated at 37 °C for 100 min and then subjected to the absorption measurements).

by using the linear calibration equation. Various volumes of the standard HAase were added into the corresponding vials to obtain the different final concentrations (1.0, 2.0 and 5.0 U/mL). Then the concentrations of HAase in urine specimens were studied based on the same procedure as mentioned above.

3. Results and discussion

3.1. UV analysis

All chemical species interact with the external light inputs and we are able to establish the relationship between absorbed energy and characteristic structural changes by measuring the absorption spectra. Herein, the UV–vis absorption curves of TPE-$4N^+$, TPE-HA and TPE-HA + HAase were studied in aqueous solution. As provided in Fig. 2A, TPE-$4N^+$ have two absorption bands centered at 286 and 363 nm, which are attributed to the π-π* local electron transitions of the phenyl and pyridine rings conjugate system. After HA was added into the solution of TPE-$4N^+$, the absorption peak corresponding to the TPE-$4N^+$ at 286 nm was decreased slightly and the peak at 363 nm gave rise to a slight blue-shift to 354 nm which might be derived from the formation of TPE-HA nano-aggregates. In the presence of HAase at different concentrations, the absorption peak at 354 nm decreased dramatically. The band at 286 nm was shifted to a short wavelength of 277 nm and the intensity gradually increased (Fig. 2B). The collected results suggested that the hydrolysis of HA might induce the disassembly of nanostructures.

3.2. Fluorescence studies

In general, the solution studies will facilitate the fundamental exploration of photophysical processes at molecular level. Luminescence signal is closely related to molecular aggregation status and emission is frequently quenched at high concentrations. The fluorescence feature of the TPE-$4N^+$ in the solution state was investigated by the steady state fluorescence spectroscopy. As shown in Fig. 3, TPE-$4N^+$ showed intense yellow emission at 580 nm in pure DMSO, which was caused by the intramolecular charge transfer (ICT) [24]. When the water content was increased, the emission intensity of TPE-$4N^+$ was suppressed step by step. At a high water fraction (99.9%), the light emission was almost quenched. However, further aggregation significantly improved emission efficiency of the organic chromophore. As described in Fig. S3, TPE-$4N^+$ was weakly emissive in its dilute aqueous solution. Its powder material demonstrated bright yellow luminescence under irradiation at 365 nm. This was considered to be caused by aggregation formation and an increase in luminescence outputs was achieved [25].

The assembly between TPE-$4N^+$ and HA was also investigated by spectrometric titration. As shown in Fig. S4, TPE-$4N^+$ (1 μM) was faintly emissive at 580 nm due to its excellent water solubility. After the addition of HA solution (0.05 μg mL^{-1}), TPE-$4N^+$ can react with HA to form the uniform nanoparticles through electrostatic interaction. The evolution of the spectra clearly manifested the fast growth of the yellow band and the peak wavelength gave rise to a blue shift from 580 to

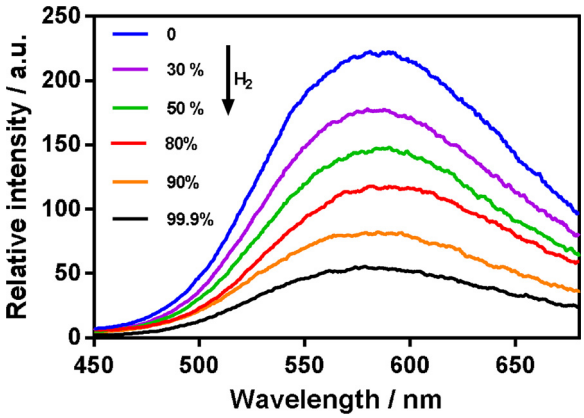

Fig. 3. Fluorescence emission spectra of TPE-$4N^+$ (1 μM) in mixture of DMSO/water with increasing fraction of water (The measurements were performed at 25 °C).

536 nm. The enhancement of luminescence indicated the nano-aggregates were well-formed. Upon the titration of HA from 0 to 0.3 μg mL^{-1}, the maximum emission value could be reached in the presence of 0.15 μg mL^{-1} of HA.

3.3. Detection of HAase

As given in Fig. S5, the chromaticity coordinate (0.351, 0.495) of the prepared sample is located at the yellow light region. Therefore, 0.15 μg mL^{-1} of HA was chosen to add in TPE-$4N^+$ solution (1 μM) for the study of enzymatic reaction between HAase and HA. Firstly, the kinetics of enzymatic reaction was performed by estimating the time-dependent emission changes of TPE-HA with the 5 U/mL of HAase (Fig. S6). The fluorescence intensities of TPE-HA were gradually decreased and reached its minimum value within 100 min upon addition of HAase (5 U/mL). This effect showed that the enzymatic time is another significant factor during the HAase detection [26]. Secondly, to ensure the enzymolysis was carried out completely, the incubation time (100 min.) was employed in the following study. As shown in Fig. 4, the photoluminescence intensity of the TPE-HA decreased based on the increasing concentration of HAase (0–5 U/mL) due to the disassembly of TPE-HA. The emission intensity of TPE-HA was nearly quenched 90% upon adding HAase (5 U/mL). The relative intensity of TPE-HA at 536 nm (F/F_0) was decreased upon addition various concentrations of HAase (from 0 to 5 U/mL) (F_0 represented initial fluorescence emission intensity of TPE-HA (TPE-$4N^+$ 1 μM, HA 0.15 μg mL^{-1}) in aqueous solution, F represented fluorescence emission intensity of TPE-HA upon addition various concnetrtions HAase). The linear regions were analyzed by two sections varying from 0.05 to 2 U/mL ($y = 0.009 - 0.418\times$ ($R^2 = 0.985$)) and from 2.75 to 5 U/mL ($y = 0.001 - 0.036\times$ ($R^2 = 0.998$)), respectively (Fig. 5). Using the first linear equation ($y = 0.009 - 0.418\times$), the detection limit for HAase was estimated to be 0.02 U/mL according to the equation DL = 3 × SD/slope, where SD is the standard deviation of the blank sample.

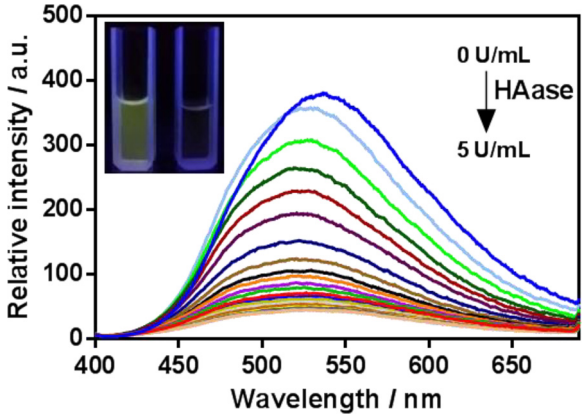

Fig. 4. Fluorescence emission spectra of TPE-HA (TPE-4N$^+$ 1 μM, HA 0.15 μg mL^{-1}) in aqueous solution after the addition of HAase (0–5 U/mL) (All the samples were incubated at 37 °C for 100 min and then subjected to the fluorescence measurements). Inset: TPE-HA (TPE-4N$^+$ 1 μM, HA 0.15 μg mL^{-1}) in aqueous solution excited by UV light at 365 nm without (left) and with (right) HAase (5 U/mL).

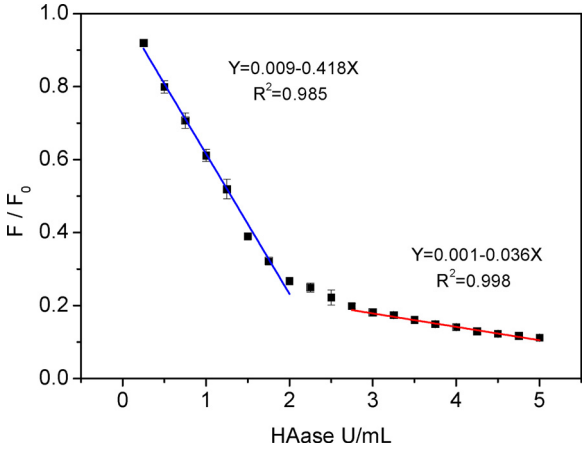

Fig. 5. Plot of the relative intensity at 536 nm (F/F_0) against various HAase concentrations (from 0 to 5 U/mL), (F_0 means initial emission intensity of TPE-HA (TPE-4N$^+$ 1 μM, HA 0.15 μg mL^{-1}) in aqueous solution, F means emission intensity of TPE-HA in the presence of different concnetrtions of HAase), (Equation for blue line: Y refers to F/F_0, X refers to concentration of HAase (ranging from 0.05 to 2 U/mL); Equation for red line: Y refers to F/F_0, X refers to concentration of HAase (ranging from 2.75 to 5 U/mL)). All data represent mean ± SD for three separate measurements. (For interpretation of the references to colour in this figure legend, the reader is referred to the web version of this article).

3.4. Selectivity experiments

To study the selectivity of TPE-HA for HAase, fluorescence responses to other 13 kinds of representative species were examined. The reference samples included GSH, Cys, Hcy, Glu, AA, ALP, UA, VB1, BSA, $CuCl_2$, $FeCl_3$, $ZnCl_2$ and $MgCl_2$. As shown in Fig. 6, only the addition of HAase induced a significant decrease of the emissive spectra at 536 nm. All the other interference species have led to no extraordinary changes and the variation in intensity was less than 5%. These results supported that the TPE-HA probe was selective for efficient recognition of HAase in aqueous solution. Therefore, this strategy of assembly-disassembly based on AIE nanosensor could be potentially employed for monitoring new targets.

3.5. Mechanism for the recognition of HAase in the sensing system

With the purpose of exploring the detection mechanism for the

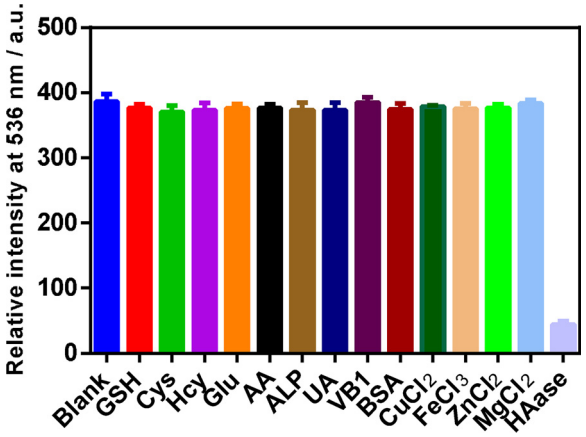

Fig. 6. Fluorescence responses of TPE-HA (TPE-4N$^+$ 1 μM, HA 0.15 μg mL^{-1}) toward different potentially interference species. (The concentrations of GSH, Cys, Hcy, Glu, AA, UA, VB1, BSA, $CuCl_2$, $FeCl_3$, $ZnCl_2$ and $MgCl_2$ are the same (10.0 μM), ALP (0.1 U/mL), and HAase (5 U/mL). All the samples were incubated at 37 °C for 100 min and then subjected to the fluorescence measurements).

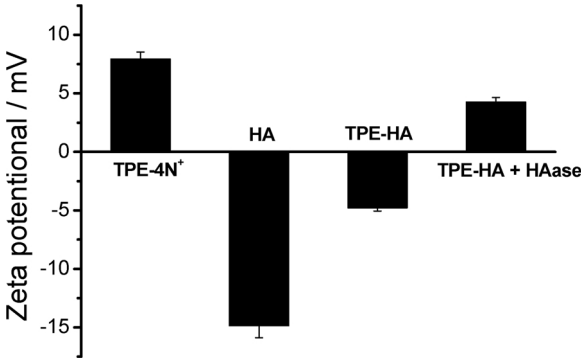

Fig. 7. Zeta potentional of TPE-4N$^+$ (1 μM), HA (0.15 μg mL^{-1}), TPE-HA (TPE-4N$^+$ 1 μM, HA 0.15 μg mL^{-1}), and TPE-HA (TPE-4N$^+$ 1 μM, HA 0.15 μg mL^{-1}) + HAase (5 U/mL) in aqueous solution (All the measurements were carried out at 25 °C).

HAase in the sensing system, the assembly and degradation of TPE-HA nano-aggregates was characterized via zeta potential measurements. The combination between TPE-4N$^+$ and HA was further verified by potential signal changes. Fig. 7 showed that the zeta potential of TPE-4N$^+$ (1 μM) was determined to be + 8.1 mV. On the contrary, the zeta potential of HA (0.15 μg mL^{-1}) was measured as −14.5 mV under the same conditions. However, when HA (0.15 μg mL^{-1}) was added into the TPE-4N$^+$ (1 μM) solution, the zeta potential of the system was decreased to -4.8 mV, indicating electrostatic attraction between the positively-charged TPE-4N$^+$ and negatively-charged HA induced the formation of aggregation. In the following step, HAase was incorporated into TPE-HA solution, the zeta potential of the system was increased to + 4.3 mV, which further proved the degradation of TPE-HA nano-aggregates [27–30].

To further clarify the sensing process, transmission electron microscopy (TEM) of TPE-4N$^+$, TPE-HA and TPE-HA + HAase were explored. As given in Fig. 8A, TPE-4N$^+$ obtained in this study was homogeneously dispersed in the form of ultra-small nanoparticles with average diameter of 5.9 nm by selecting 100 samples (Fig. S7A). After adding HA into TPE-4N$^+$ solutions, the negatively charged HA can react with TPE-4N$^+$ to trigger the formation of the large aggregated nanoparticles and regular spherical particles with the average diameter of 170.5 nm were obtained (Fig. 8B and S7B). The morphology evolution indicated TPE-HA nano-aggregates were facilely established through their electrostatic interaction. Moreover, the particle size

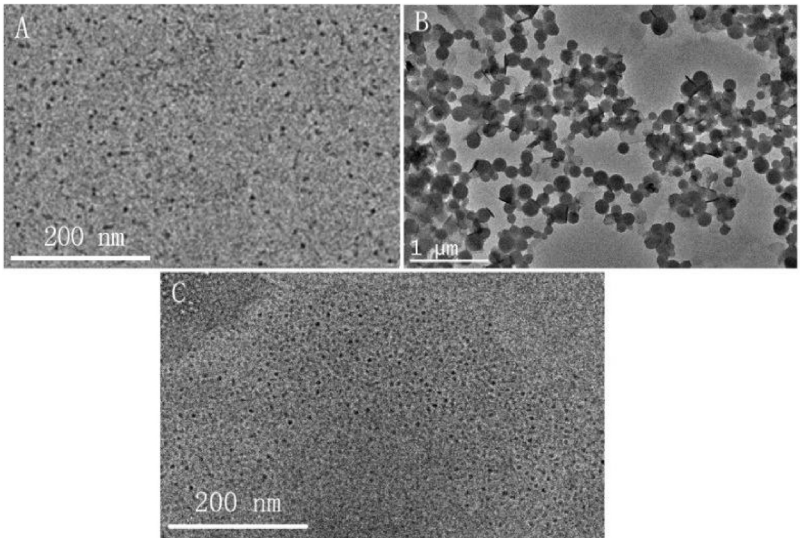

Fig. 8. TEM images of (A) TPE-4N$^+$, (B) TPE-HA and (C) TPE-HA + HAase. (10 μL aqueous solution samples A (TPE-4N$^+$ (1 μM)), B (TPE-HA (TPE-4N$^+$ 1 μM, HA 0.15 μg mL^{-1})) and C (TPE-HA (TPE-4N$^+$ 1 μM, HA 0.15 μg mL^{-1}) + HAase (5 U/mL)) were dropped onto a carbon-coated copper grid for TEM observations).

distribution of TPE-HA was achieved in its dynamic light scattering (DLS) histogram (Fig. S8). Interestingly, in the same reaction system, the addition of HAase could promote the decomposition of the aggregated nanostructures and the uniform particles with a diameter of 6 nm was found again (Fig. 8C and S7C). The results supported that the enzymatic hydrolysis of hyaluronic acid could drastically change the charge distribution of the sensor system and degrade the nano-aggregates of TPE-HA [31–34]. HAase-controlled disassembly in water at ambient temperature will offer an alternative and useful way for microstructure design of various nanocrystals.

3.6. Analyzing HAase in urine samples

To gain further insights into the practical applicability of TPE-HA, urine samples spiked with fixed HAase concentrations were assayed. Human urine specimens from two healthy people were collected and analyzed to support its validity. Table S1 demonstrated the concentrations of HAase in urine samples for the normal healthy people and the determined levels were much lower than the reported data for the patients [28]. To investigate the recovery efficiency for the HAase in urine specimens, the solution was added with appropriate amounts of HAase (1.0, 2.0 and 5.0 U/mL) and the final measured concentrations in all samples were given in Table S1. The average recoveries of HAase were in the range of 97–108 % for all the spiked samples and low relative standard deviation (0.95–1.08 %) was achieved. The collected data will meet the requirement for future practical use. These new findings may contribute to the assembly of novel molecular engineering works that could be adaptable to the utilizations in real samples.

4. Conclusions

In this research, a highly sensitive and selective probe for the detection of hyaluronidase has been achieved based on the AIE principle. The sensing mechanism of TPE-HA towards HAase was established on electrostatic interaction. The detailed processes were supported by the zeta potential measurements, transmission electron microscopy and particle size analysis. This new route for the quantitative determination of HAase possesses a few advantages. As for the synthesis strategy, the probe TPE-4N$^+$ can be easily prepared within one step and no painstaking operation is needed. In addition, the detection of HAase can be applied in aqueous solution or buffer environment. Furthermore, the interference of HAase would be avoided. Therefore, it is expected that this AIE-based nanostructure could be integrated into suitable hosts for practical diagnosis and treatment of HAase-derived diseases.

Acknowledgments

Q. M. acknowledges the support from National Natural Science Foundation of China (21371063) and Guangdong Science and Technology plan (2016A050502053). Z. Z. acknowledges the Scientific Research Fund of Henan Provincial Education Department (17A150016) and Natural Science Foundation of Henan (162300410200) for financial assistances. Y. H. thanks Research fund of higher education committee of Guangdong province (GDJ2016003). J.W. is grateful to the support from Innovation team project by department of Education of Guangdong Province (2016KCXTD009).

Appendix A. Supplementary data

Supplementary material related to this article can be found, in the online version, at doi:https://doi.org/10.1016/j.snb.2018.08.093.

References

[1] W.Q. Yang, J.C. Ni, F. Luo, W. Weng, Q.H. Wei, Z.Y. Lin, G.N. Chen, Cationic carbon dots for modification-free detection of hyaluronidase via an electrostatic-controlled ratiometric fluorescence assay, Anal. Chem. 89 (2017) 8384–8390.
[2] Y.N. Zhong, F.H. Meng, C. Deng, Z.Y. Zhong, Ligand-directed active tumor-targeting polymeric nanoparticles for cancer chemotherapy, Biomacromolecules 15 (2014) 1955–1969.
[3] C. Kolliopoulos, D. Bounias, H. Bouga, D. Kyriakopoulou, M. Stavropoulos, D.H. Vynios, Hyaluronidases and their inhibitors in the serum of colorectal carcinoma patients, J. Pharmaceut. Biomed. 83 (2013) 299–304.
[4] E. Sanaa, S. Hanan, M. Amal, E. Mohamed, E.A. Omar, Detection of hyaluronidase RNA and activity in urine of schistosomal and non-schistosomal bladder cancer, Med. Oncol. 29 (2012) 3345–3351.
[5] I.D. Ferrante, Turbidimetric measurement of acid mucopolysaccharides and hyaluronidase activity, J. Biol. Chem. 22 (1956) 303–306.
[6] K.P. Vercruysse, A.R. Lauwers, J.M. Demeester, bsolute and empirical determination of the enzymic activity and kinetic investigation of the action of hyaluronidase on hyaluronan using viscosimetry, Biochem. J. 306 (1995) 153–160.
[7] R.R. Li, Q.L. Yu, L. Han, L.Y. Rong, M.M. Yang, M.R. An, Isolation and enzymatic characterization of the first reported hyaluronidase from Yak (Bos grunniens) testis, Korean J. Chem. Eng. 31 (2014) 2027–2034.
[8] J.D. Luo, Z.L. Xie, J.W.Y. Lam, L. Cheng, H.Y. Chen, C.F. Qiu, H.S. Kwok, X.W. Zhan, Y.Q. Liu, D.B. Zhu, B.Z. Tang, Aggregation-induced emission of 1-methyl-1,2,3,4,5-pentaphenylsilole, Chem. Commun. 0 (2001) 1740–1741.
[9] A.J. Qin, B.Z. Tang, Aggregation-induced emission: fundamentals and applications, Energ. Build. 35 (2013) 933–940.
[10] J. Wang, J. Mei, R.R. Hu, J.Z. Sun, A.J. Qin, B.Z. Tang, Click synthesis, aggregation-induced emission, E/Z isomerization, self-organization, and multiple chromisms of pure stereoisomers of a tetraphenylethene-cored luminogen, J. Am. Chem. Soc. 134

(2012) 9956–9966.
[11] Z.L. Zhang, R.T.K. Kwok, Y. Yu, B.Z. Tang, K.M. Ng, Sensitive and specific detection of L-lactate using an AIE-active fluorophore, ACS Appl. Mater. Interfaces 9 (2017) 38153–38158.
[12] H.F. Xie, F. Zeng, S.Z. Wu, Ratiometric fluorescent biosensor for hyaluronidase with hyaluronan as both nanoparticle scaffold and substrate for enzymatic reaction, Biomacromolecules 15 (2014) 3383–3389.
[13] B.P. Jiang, X. Tan, X.C. Shen, W.Q. Lei, W.Q. Liang, S.C. Ji, H. Liang, One-step fabrication of a multifunctional aggregation-induced emission nanoaggregate for targeted cell imaging and enzyme triggered cancer chemotherapy, ACS Macro Lett. 5 (2016) 450–454.
[14] G.Y. Jiang, G.J. Zeng, W.P. Zhu, Y.D. Li, X.B. Dong, G.X. Zhang, X.L. Fan, J.G. Wang, Y.Q. Wu, B.Z. Tang, A selective and light-up fluorescent probe for β-galactosidase activity detection and imaging in living cells based on an AIE tetraphenylethylene derivative, Chem. Commun. 53 (2017) 4505–4508.
[15] C.Y.K. Chan, Z. Zhao, J.W.Y. Lam, J. Liu, S. Chen, P. Lu, F. Mahtab, X. Chen, H.H.Y. Sung, H.S. Kwok, Y. Ma, I.D. Williams, K.S. Wong, B.Z. Tang, Adv, Funct. Mater. 22 (2012) 378–389.
[16] Y.H. Xu, L. Chen, Z.Q. Guo, A. Nagai, D.L. Jiang, Light-emitting conjugated polymers with microporous network architecture: interweaving scaffold promotes electronic conjugation, facilitates exciton migration, and improves luminescence, J. Am. Chem. Soc. 133 (2011) 17622–17625.
[17] M. Wang, Y.R. Zheng, K. Ghosh, P.J. Stang, Metallosupramolecular tetragonal prisms via multicomponent coordination-driven template-free self-assembly, J. Am. Chem. Soc. 132 (2010) 6282–6283.
[18] X.R. Wang, J.M. Hu, T. Liu, G.Y. Zhang, S. Liu, Highly sensitive and selective fluorometric off-on K^+ probe constructed via host-guest molecular recognition and aggregation-induced emission, J. Mater. Chem. 22 (2012) 8622–8628.
[19] Y.S. Li, A.D. Shao, Y. Wang, J. Mei, D.C. Niu, J.L. Gu, P. Shi, W.H. Zhu, H. Tian, J.L. Shi, Morphology-tailoring of a red AIEgen from microsized rods to nanospheres for tumor-targeted bioimaging, Adv. Mater. 28 (2016) 3187–3193.
[20] G.Y. Jiang, X. Liu, Q.Q. Chen, G.J. Zeng, Y.Q. Wu, X.B. Dong, G.X. Zhang, Y.D. Li, X.L. Fan, J.G. Wang, A new tetraphenylethylene based AIE probe for light-up and discriminatory detection of Cys over Hcy and GSH, Sensors Actuators B 252 (2017) 712–716.
[21] Z. Zhou, F.L. Gu, L. Peng, Y. Hua, Q.M. Wang, Spectroscopic analysis and in vitro imaging applications of a pH responsive AIE sensor with a two-input inhibit function, Chem. Commun. 51 (2015) 12060–12063.
[22] H.B. Fang, G.M. Cai, Y. Hu, J.Y. Zhang, Tetraphenylethylene-based acylhydrazone gel for selective luminescent sensing, Chem. Commun. 54 (2018) 3045–3048.
[23] C. Wang, H.Y. Ji, M.S. Li, L.K. Cai, Z.P. Wang, Q.Q. Li, Z. Li, A highly sensitive and selective fluorescent probe for hypochlorite in pure water with aggregation induced emission characteristics, Faraday Discuss. 196 (2017) 427–438.
[24] H.R. Xu, K. Li, S.Y. Jiao, S.L. Pan, J.R. Zeng, X.Q. Yu, Tetraphenylethene-pyridine salts as the first self-assembling chemosensor for pyrophosphate, Analyst 140 (2015) 4182–4188.
[25] H.C. Ma, M.Y. Yang, C.L. Zhang, Y.C. Ma, Y.F. Qin, Z.Q. Lei, L. Chang, L. Lei, To Wang, Y. Yang, Aggregation-induced emission (AIE)-active fluorescent probes with multi-binding sites toward ATP sensing and the live cell imaging, J. Mater. Chem. B 5 (2017) 8525–8531.
[26] Q.H. Hu, F. Zen, S.Z. Wu, A ratiometric fluorescent probe for hyaluronidase detection via hyaluronan-induced formation of red-light emitting excimers, Biosens. Bioelectron. 79 (2016) 776–783.
[27] Z. Wang, X.H. Li, Y.C. Song, L.H. Li, W. Shi, H.M. Ma, An upconversion luminescence nanoprobe for the ultrasensitive detection of hyaluronidase, Anal. Chem. 87 (2015) 5816–5823.
[28] D. Cheng, W.Y. Han, K.C. Yan, Y. Song, M.D. Jiang, E.Q. Song, One-step facile synthesis of hyaluronic acid functionalized fluorescent gold nanoprobes sensitive to hyaluronidase in urine specimen from bladder cancer patients, Talanta 130 (2014) 408–414.
[29] N. Gao, W. Yang, H.L. Nie, Y.Q. Gong, J. Jing, L.J. Gao, X.L. Zhang, Turn-on theranostic fluorescent nanoprobe by electrostatic self-assembly of carbon dots with doxorubicin for targeted cancer cell imaging, in vivo hyaluronidase analysis, and targeted drug delivery, Biosens. Bioelectron. 96 (2017) 300–307.
[30] K. Wang, J.H. Cui, S.Y. Xing, X.W. Ren, Hyaluronidase/temperature dual-responsive supramolecular assembly based on the anionic recognition of calixpyridinium, Chem. Commun. 53 (2017) 7517–7520.
[31] K.C. Yang, M.X. Liu, Y.Y. Wang, S.S. Wang, H. Miao, L.Q. Yan, X.M. Yang, Carbon dots derived from fungus for sensing hyaluronic acid and hyaluronidase, Sens. Actuators B 251 (2017) 503–508.
[32] A.I. Nossier, S. Eissa, M.F. Ismail, M.A. Hamdy, H.M.E. Azzazy, Direct detection of hyaluronidase in urine using cationic gold nanoparticles: a potential diagnostic test for bladder cancer, Biosens. Bioelectron. 54 (2014) 7–14.
[33] W.J. Li, C.F. Zheng, Z.Y. Pan, C. Chen, D.L. Hu, G.H. Gao, S.D. Kang, H.D. Cui, P. Gong, L.T. Cai, Smart hyaluronidase-actived theranostic micelles for dual-modal imaging guided photodynamic therapy, Biomaterials 101 (2016) 10–19.
[34] W. Gu, Y.H. Yan, C.L. Zhang, C.P. Ding, Y.Z. Xian, One-step synthesis of water-soluble MoS_2 quantum dots via a hydrothermal method as a fluorescent probe for hyaluronidase detection, ACS Appl. Mater. Interfaces 8 (2016) 11272–11279.

Xiangqian Li received his bachelor degree from Hengyang Normal University in 2016, China. Currently he is pursuing for doctor degree under the supervision of Prof. Qianming Wang in South China Normal University. His research interests focus mainly on the development of optical sensors and devices.

Zhan Zhou obtained his bachelor degree in chemistry department of Shang Qiu Normal University, Henan, China (July, 2010). In December of 2015, he received his doctor degree from South China Normal University under the supervision of Prof. Qianming Wang. From May of 2016, he became an assistant Professor in Luoyang Normal University. His current research interests include the synthesis and assembly of smart lanthanide luminescent sensors.

Yiping Tang Engineering from Zhejiang University of Technology. His studies are focused on the design of novel metallic functional materials and their applications.

Cheng Cheng Zhang received his PhD degree from University of Illinois at Urbana-Champaign (USA) in year 1999. He became a postdoctoral fellow in Massachusetts Institute of Technology from 2000 to 2006 under the tutelage of Professor Harvey F. Lodish. He currently holds the Morton H. Sanger Professorship in Oncology at UT Southwestern Medical Center. He has gained numerous prizes and awards, most recently being selected as Michael L. Rosenberg Scholar in Biomedical Research and won Royan International Research Award in year 2012. He has contributed more than 100 peer-reviewed articles in well-known international journals and books.

Yuhui Zheng was educated at Nanchang Hangkong University, (Nanchang, P. R. China) and received her master degree in June. 2009. She has carried out the research work concerning molecular design and materials assembly in the field of photochemistry. She has joined in Professor Wang's team in South China Normal University (Guangzhou, P. R. China) since March of 2010. From December of year 2013, she has been promoted to Associate Professor. Her research addresses problems at the interfaces of lanthanide molecular complexes, nanomaterials, biosensors and optoelectronics.

Jinwei Gao is a full professor of Guangdong Provincial Engineering Technology Research Center For Transparent Conductive Materials in South China Normal University. His current research includes synthesis and preparation of transparent electrodes and design of responsive hybrid materials.

Qianming Wang received a bachelor degree in Applied Chemistry from Xiangtan University (P. R. China) in 2000. He studied for his PhD degree at Tongji University (Shanghai, P. R. China) under the supervision of Professor Bing Yan until the end of year 2006. After staying as a postdoctoral fellow in Italy and Japan for nearly three years, he started his own work in South China Normal University from September of 2009. He was promoted to full professor in May of 2010. His research interests include lanthanide-based hybrid materials, probes, nanomedicine and sensor engineering.